HIGH CURRENT HARMONIC CONTROL STRATEGY FOR A T-NPC INTERLEAVED AC ACTIVE ELECTRONIC POWER LOADS

Alisson Mengatto[1], Felipe J. Zimman[1], Joselito A. Heerdt[1]
[1]Santa Catarina State University - UDESC, Joinville – SC, Brazil
e-mail: dee6am@joinville.udesc.br, felipezimann@hotmail.com, joselito.heerdt@udesc.br

***Abstract* – The project of controllers for an AC Active Electronic Power Load capable of emulating non-linear currents brings some challenges, like the necessity of high performance controllers and damping of the resonant coupling filter with the Equipment Under Test. On the other hand, high dynamic controllers require high switching frequencies in a Pulse Width Modulation, but power semiconductors with high currents and high frequency capabilities are difficult to obtain. In this paper, it is proposed a control strategy for the T-Type Neutral Point Clamped Interleaved Converter in a single-phase active electronic load application. State observer and state feedback in addition with classic controller are used for high current harmonics tracking. The control oriented modeling and the control system design are presented. Simulation and experimental results obtained from a 10 kW single-phase three-level converter prototype illustrate and demonstrate the feasibility of the proposed control strategy.**

***Keywords* – Active Electronic Load, current harmonic control, state feedback fontroller, T-Type NPC.**

I. INTRODUCTION

Worldwide, people think of reducing the environmental impact and provide savings of energy through more efficient products and solutions. The use of passive loads in burn-in routines or in maintenances on Equipment Under Test (EUT), mainly for high power, are unviable. Alternated Current Active Electronic Loads (AC AEL) are capable to regenerate the energy demanded by EUT on the grid through a back-to-back converter, bringing cost and volume reduction, flexibility, besides reducing concerns over thermal management caused by passive loads heat dissipation.

AEL are also known in the literature as Energy Recycles, [1], Virtual Loads (VL) [2], Load Emulators [3], and they are employed in tests of measurement equipment, uninterruptible power supplies (UPS), voltage sources, power transformers, among other applications. Furthermore, the capability of emulating different loads can be applied in drives for industrial motors [4], wind turbines [5], and electrical vehicles [6], and also, imitating solar panels dynamics [7]. Figure 1 shows the proposed AC AEL system.

The rectifier converter is responsible to tracking the reference current of the system being emulated and attenuate a possible filter resonance with the leakage inductance of the EUT, so, must have a very fast response. The inverter has the function of controlling the bus voltage and providing a sinusoidal current back to the grid.

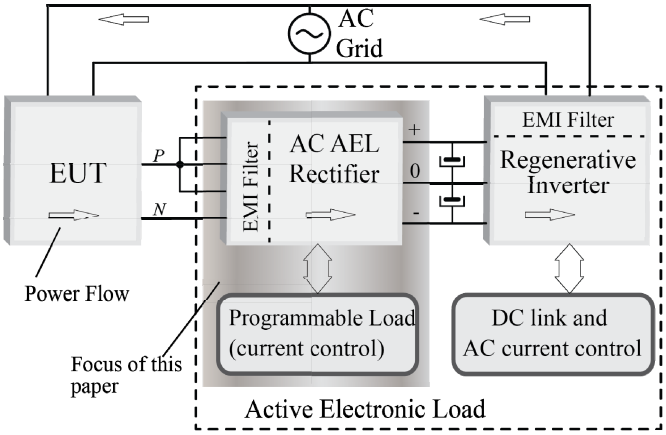

Fig. 1. Block diagram of proposed regenerative AEL system.

Unfortunately, the control strategy design for an AEL presents some challenges. The current control of high order harmonics demands high dynamic controllers, which in turn, require higher sampling and switching frequencies.

This work proposes a control strategy for the rectifier converter. In order to obtain a higher power density operating in single phase, the AEL is based on a three-phase-level T-Type Neutral-Point-Clamped (T-NPC) converter [8, 9] with the phases connected in parallel as illustrated in Figure 2a). This arrangement benefits cases where is necessary emulate high power loads for single phase EUTs, with the facility of simply changing the controller of a three-phase converter and connecting its input in parallel. Interleaving the phases adds another benefit to this configuration, reducing the input current ripple by a factor of three.

Considering the inductance of EUT, the resulting coupling filter is the LCL type, and brings added difficulty for the controller due to its characteristic resonance, with the advantage of high attenuation of switching frequencies [10].

The final objective is to reproduce a given current harmonic profile with high amplitude and low ripple, and the applications focus are single-phase transformers or uninterruptible power supplies testing that are subject to heavy harmonic pollution.

II. SYSTEM MODELING

The converter model is obtained following the procedure described in [11]. Inverter voltage is considered as a controlled voltage source with a respective series inductor per phase. Each positive and negative dc link voltages are considered regulated and balanced in the value of *E/2*. In this work, although there is carrier displacement, the same duty cycle function is imposed for the three converter legs. Therefore, in

978-1-4799-8779-5/15/$31.00 ©2015 IEEE

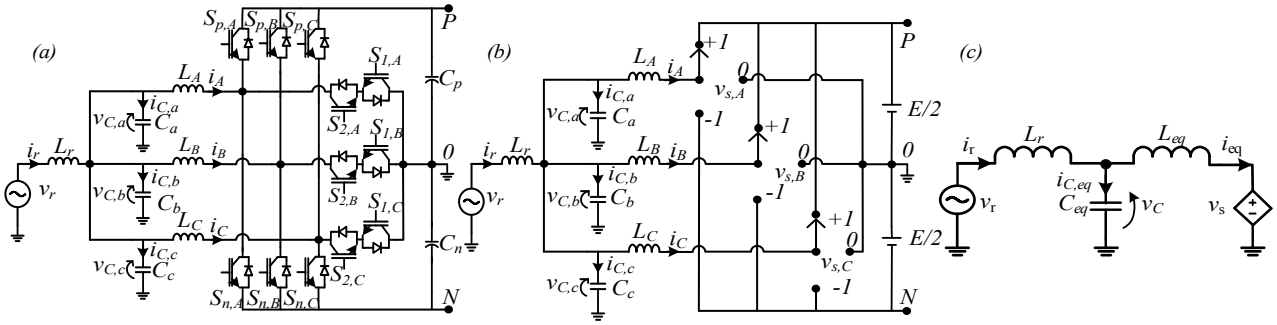

Fig. 2. Proposed interleaved T-Type NPC: a) System connection; b) Three-state switching model; c) Simplified model

Figure 2b), $v_{s,A} = v_{s,B} = v_{s,C}$ and the average value in a switching period of v_s, is defined as $v_s = d(t).E/2$, where $d(t)$ is the duty cycle function and varies from -1 to 1.

Assuming $v_{s,i}$ voltages are the same, it can be considered that the converter side inductors are connected in parallel, so,

$$i_{eq} = i_A + i_B + i_C \qquad L_{eq} = \left(\frac{1}{L_A} + \frac{1}{L_B} + \frac{1}{L_C} \right)^{-1} \qquad (1)$$
$$i_{C,eq} = i_{C,a} + i_{C,b} + i_{C,c} \qquad C_{eq} = C_a + C_b + C_c$$

where i_{eq}, $i_{C,eq}$, L_{eq}, e C_{eq} are respectively, the equivalent converter side current, current through filter capacitor, equivalent inductance and capacitance. The simplified model is showed in Figure 2c). Choosing the state vectors as $x = \begin{bmatrix} i_r & i_{eq} & v_C \end{bmatrix}^T$, the input vectors $u = \begin{bmatrix} v_r & d \end{bmatrix}^T$, and the EUT current as control object, the average state space representation is given by $\dot{x} = Ax + Bu$ and $y = Cx$, where,

$$A = \begin{bmatrix} 0 & 0 & \frac{-1}{L_r} \\ 0 & 0 & \frac{1}{L_{eq}} \\ \frac{1}{C_{eq}} & \frac{-1}{C_{eq}} & 0 \end{bmatrix} \quad B = \begin{bmatrix} B_1 \mid B_2 \end{bmatrix} = \left[\begin{array}{c|c} \frac{1}{L_r} & 0 \\ 0 & \frac{-E}{2L_{eq}} \\ 0 & 0 \end{array}\right] \qquad (2)$$

State feedback and observer are performed in discrete time domain [12]. The state matrix, considering sampled period T, become as showed in (3) and its discretization is presented in (4).

$$A_d = e^{AT}, \quad B_d = \begin{bmatrix} B_{d1} \mid B_{d2} \end{bmatrix} = \left(\int_0^T e^{AT} dt \right) B \qquad (3)$$

$$\begin{bmatrix} i_r(k+1) \\ i_{eq}(k+1) \\ v_c(k+1) \end{bmatrix} = A_d x(k) + B_{d1} v_r(k) + B_{d2} d(k), \quad y = Cx(k) \qquad (4)$$

EUT voltage (v_r) is considered constant on each sampling interval k, as its interval is much smaller than grid period.

III. CONTROL DESIGN

The control strategy aims to modify the plant poles, allowing active damping of the resonance [10]. Furthermore, a classical controller is inserted to improve tracking current response and disturbance rejection. EUT current is not measured, but estimated through state observer. The *LCL* filter resonance is actively damped through a state feedback technique [13]. Considering v_r as a perturbation rejected by the classical controller, the new system dynamic equation is

$$x(k+1) = (A_d - B_{d2}K)x(k) + B_{d1}v_r(k) + B_{d2}i_r^*(k) \qquad (5)$$

The gains vector K that lead the plant poles to the specified position in z-plane (p_1, p_2, p_3), is obtained through the characteristic equation. The plant magnitude, with and without state feedback, is illustrated in Figure 3 by the Bode diagram and shows the new steady state response behavior of input current (i_r). Figure 4 shows the pole mapping done in z-plane considering a variation of vector K.

A. State and Observer Feedback

Pure proportional state feedback yields steady state errors [14] and to obtain high capacity of tracking current reference supplied by EUT, and at the same time reject its disturbance voltage, a controller is added considering that state feedback is already stabilized, therefore with slower dynamic. With the state feedback system approximated by Tustin's bilinear method in the w-plane [15] it is possible to get the specifications in frequency domain, obtained by (6), where I is the identity matrix.

$$G(z) = \frac{i_r(z)}{i_r^*(z)} = C(zI - A_d + \mathrm{B}_{d2}K)^{-1} B_{d2} \qquad (6)$$

Efficient current tracking is obtained using a PI controller with double integrator, given in w-plane domain by (7)

$$C(w) = k_c \frac{w^2 + b_1 w + b_2}{w^2} \qquad (7)$$

The open loop Bode diagram is presented in Figure 5 and is applied on the state feedback plant. A conventional Luenberger observer was used for the EUT current (i_r) estimation. As EUT voltage is considered a perturbation, this dynamic is inserted on the observer even without measurement through its state space model given by (8)-(9). These new observer states do not change the system observability [16] and pole placement can be chosen arbitrarily in the z-plane. Proportional gains are applied on the difference between real measured and observed states in order to eliminate estimation errors through matrix L.

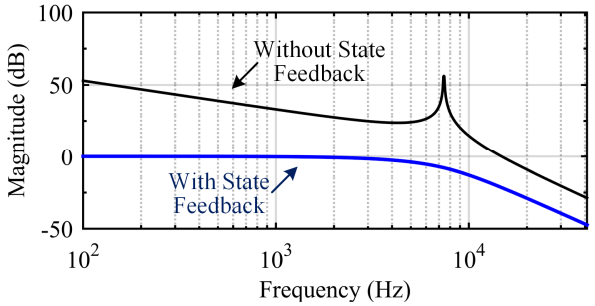

Fig. 3. - System response i_r with and without state feedback.

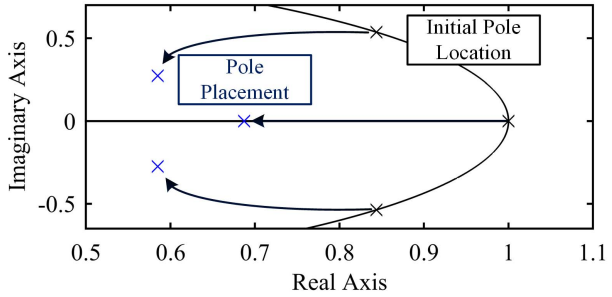

Fig. 4. Z-plane mapping and the effect of K gains variation under plant poles position.

Besides, observer is used as a predictive way to compensate the digital one sample delay of pulse width modulation (PWM) [17] comparing the next instant reference with the next sampling instant prediction of the observer. The observer model is achieved considering

$$v_r = Asen(\omega t) \quad \frac{d^2}{dt^2}v_r = -A\omega^2 sen(\omega t) = -\omega^2 v_r \qquad (8)$$

where ω is EUT voltage angular frequency. The observer state vector is $\tilde{x} = \left[\tilde{i}_r \;\; \tilde{i}_{eq} \;\; \tilde{v}_C \;\; \tilde{v}_r \;\; \frac{d}{dt}\tilde{v}_r\right]^T$, and the equivalent system, as illustrated on Figure 6, is obtained with $\dot{\tilde{x}} = A_o\,\tilde{x} + B_o d + L(C_{o,1}x - C_o\tilde{x})$, where

$$A_o = \begin{bmatrix} A_{3x3} & B_{1\,3x1} & 0_{3x1} \\ 0_{1x3} & 0 & 1 \\ 0_{1x3} & -\omega^2 & 0 \end{bmatrix} \quad B_o = \begin{bmatrix} B_{2\,3x1} \\ 0_{2x1} \end{bmatrix}$$
$$C_o = \left[C_{o,1} \mid C_{o,2}\right] = \left[\begin{array}{ccc|cc} 0 & 1 & 0 & 0 & 0 \\ 0 & 0 & 1 & 0 & 0 \end{array}\right]. \qquad (9)$$

The same discretization techniques of (3) are applied to find the discrete matrix A_o and B_o, respectively $A_{d,o}$ e $B_{d,o}$, and the discrete system is represented in (10).

$$\tilde{x}(k+1) = A_{d,o}\tilde{x}(k) + B_{d,o}d(k) + L_o(C_{o,1}x(k) - C_o\tilde{x}(k)) \quad (10)$$

The L_o matrix gains are given by pole placement, with poles 1.5 times further than the slow state feedback real pole, considering that observer must converge before, in order to avoid interaction with feedback poles.

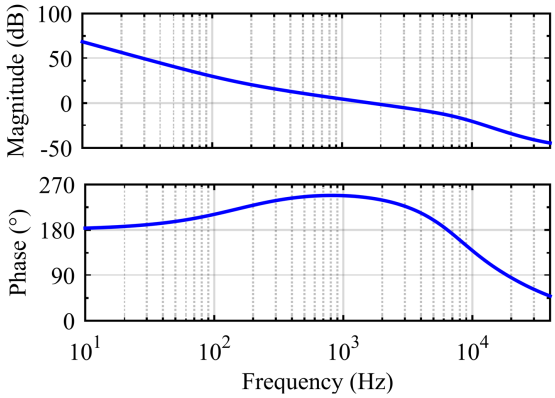

Fig. 5. Open loop bode diagram of controller with state feedback plant

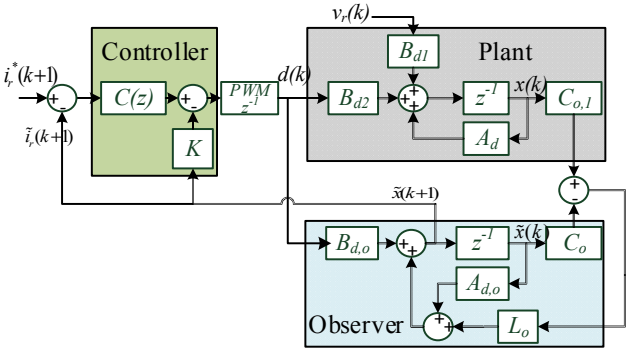

Fig. 6. Plant, controller, and observer block diagram.

IV. CONSIDERATIONS ABOUT THE INTERLEAVING

To ensure the interleaving in the simplest way, the phases in parallel of the converter was not controlled. Three independent controllers would make the use of interleaving complex, because of the three different duty cycle functions. So, to prove that the strategy adopted was able to not have a significant disbalance between the currents phases, the converter was implemented with different inductors. Phase *A* with 600μH and Phase *B* and *C* with 700μH.

The main drawbacks of this strategy are the necessity to guarantee that the duty cycle functions of the three phases are indeed almost equal and the different currents, and consequently the unequal power distribution between the phases, if the converter is implemented with different inductors. However, as the focus of this control strategy is for T-NPC three phase rectifier converters with its input connected, the requirements are satisfied, as normally the three phase implementations are homogeneous (i.e., drivers, transistors, diodes, inductors are the same between the phases). The T-NPC topology also helps, as it has a symmetrical distribution of losses in the switches [8].

V. SIMULATION RESULTS

In order to verify the models and the feasibility of the system proposed, AC AEL was simulated considering the main experimental issues. Table I and Table II presents the setup and controller parameters applied.

TABLE I
Setup Parameters

Symbol	Quantity	Value
E	DC Bus	400V
v_r	EUT Voltage	127 V_{RMS}
ω	EUT angular frequency	2π.60 rad/s
L_A - L_B, L_C	AEL side inductor	600 - 700 µH
L_r	EUT side inductor	250 to 3000µH – Nominal 500µH
C_a, C_b, C_c	AC Filter Capacitor	1 µF
f_s	Switching Frequency	40 kHz
f_a	Sampling Frequency	80 kHz

TABLE II
Controller Parameters

Symbol	Quantity	Value
fc	Crossover Frequency	1.7 *kHz*
p1, *p2*, *p3*	*z*-plane pole position	0.58 ±j0.28; 0.69
ps1, *ps2*, *ps3*	Equivalent continuos pole	5.57 ±j5.73; 4.77 *kHz*
PM	Phase Margin	62º
GM	Gain Margin	12.08 *dB*

Figure 7a) shows the comparison between the responses of real and observed currents when a step of 5A is applied on the maximum points of the sinusoidal reference. In Figure 7b), the same conditions of Figure 7a) were applied and a total equivalent current is formed by the three current phases in a carrier phase shift of 120°. These results confirm that for sinusoidal grid frequency the proposed controller was able to track the reference with an excellent response.

For a non-linear load, the simulation results of the AC AEL emulating the input current of a single-phase rectifier with capacitive filter are illustrated in Figure 7c) and Figure 7d). An 8.4% overshoot in the current peak of reference in confrontation with observed and real i_r current was verified. That is because the PI with double integrator controller tends to have greater overshoot than conventional PI in similar conditions, with the advantage to have lower steady-state error. Figure 7d) presents the response frequency comparison between reference and current response. It is noted that as the frequency increases the errors become greater, due to the bandwidth limitation of the controller.

In order to ensure that the proposed control method is valid to different values, a parametric variation of EUT inductance is done. Simulation results are showed in Figure 8 and illustrate the current response for inductance value of 250µH and 3*m*H. Although there is high overshoot of current for 3*m*H, in steady state the response presents almost zero error. For 250µH the results were satisfactory and similar to the already presented to nominal value.

VI. EXPERIMENTAL RESULTS

The experimental results are shown in Figure 9–Figure 13. Parameters of Table I are the same which are applied for the simulation setup, except the EUT inductance, which was 1*m*H approximately of a voltage variable autotransformer in the 127 RMS Volts equivalent position. To implement the proposed digital controller of AC AEL was used a DSC TMS320F28335.

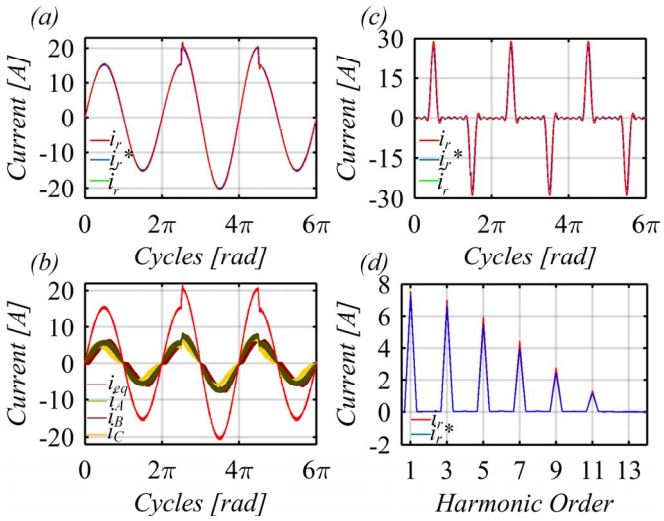

Fig. 7. Simulation results showing the efficiency of the proposed method: a) Sinusoidal current reference (i_r*), observed $(\tilde{i}_r)$ and EUT current response (i_r) with a 5A step current. *b*) Same conditions of *a)* illustrating the converter currents and its total equivalent sum. *c)* Emulation of a single-phase capacitive rectifier current reference, observed and EUT current input. *d)* Magnitude of harmonic orders of reference and input current in the same conditions of *c)*.

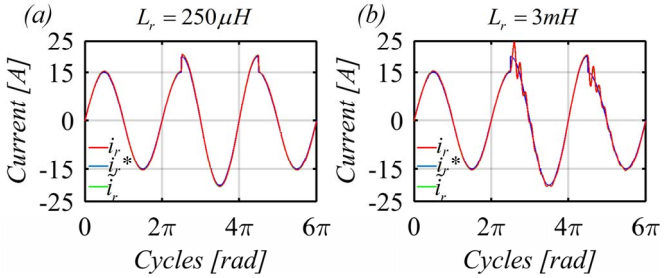

Fig. 8. Simulation results showing reference (i_r*), observed $(\tilde{i}_r)$ and EUT current response (i_r) to the parametric variation of EUT inductance for a 5A step current; a) 250µH; b) 3*m*H.

In Figure 9 the converter input voltage in phase with EUT current is illustrated, thus, emulating a resistive load. Input current was measured with THD of 1.26% even with voltage THD of 3%. These results also demonstrate that the proposed observer and controller are capable of predicting and controlling the input converter current with high accuracy and for high current operation.

Figure 10 shows the three current phases interleaved in the same conditions of Figure 9. As expected the RMS value of current in phase *A* is bigger than phase *B* and *C* due to lower value of inductance, however, a small mismatch between the average value of currents in a grid period occurs even with the input current having nearly zero average value. This is caused because the current in the inductance filter in converter side were not controlled, having little differences between switching times in each phase. This difference showed to be linear increasing the total current and acceptable for the purpose of this application. Approximating Figure 10, you can see in Figure 11 the phase shift of 120° between phases, showing the feasibility of the proposed interleaved current increasing the frequency in the input EUT filter.

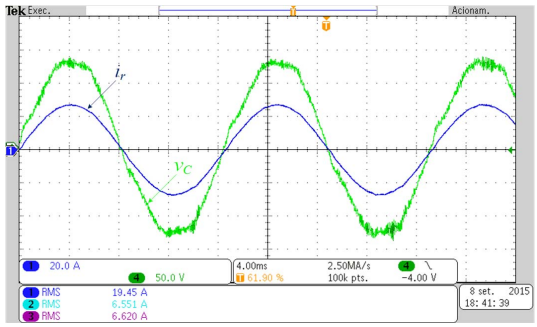

Fig. 9. Sinusoidal input experimental current emulating a resistive load. Total input current (blue, 20A/div) and input voltage (green, 50V/div) with RMS values of 19.45 Amperes and 97 Volts, respectively. Time Scale: 4*ms*/div.

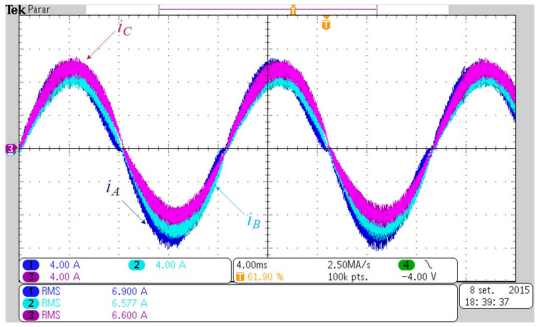

Fig. 10. Sinusoidal phase A (blue, 4A/div), B (cyan, 4A/div) and C (purple, 4A/div) converter currents. Time Scale: 4*ms*/div.

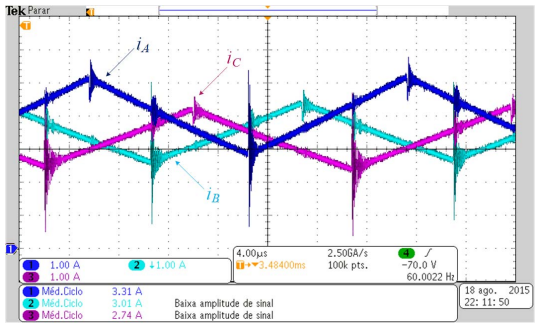

Fig. 11. Interleaved phase A (blue, 1A/div), B (cyan, 1A/div), and C (purple, 1A/div) currents on the converter inductors. Time Scale: 4μ*s*/div.

The input voltage and current of a triangular current waveform emulation are shown in Figure 12a) and in order to compare the expected and obtained frequency response of the implemented system, Figure 12b) illustrates the nearly equal reference and current amplitudes on each harmonic order of the fundamental frequency. The same is done by the emulation of the single-phase filter capacitive rectifier in Figure 13a) and Figure 13b). However, an overshoot in the zero crossing seems to distort the expected and obtained harmonic orders amplitudes. In the first case, the THD current expected was 12.11% and the experimental value was 13.41%, however, in the second, THD current expected was 131% and the experimental value was 140%.

The T-NPC prototype [18] implemented for the control strategy verification is illustrated in Figure 14.

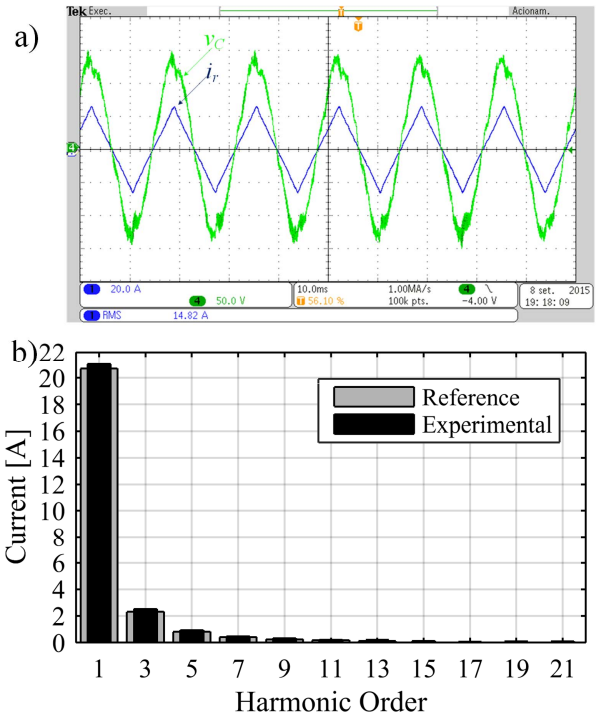

Fig. 12. Triangular waveform emulation. a) input current (blue, 20A/div) and input voltage (green, 50V/div) with RMS values of 14.82 Amperes and 109 Volts, respectively. Time Scale: 10*ms*/div; b) Harmonic amplitudes comparison among experimental and reference triangular current.

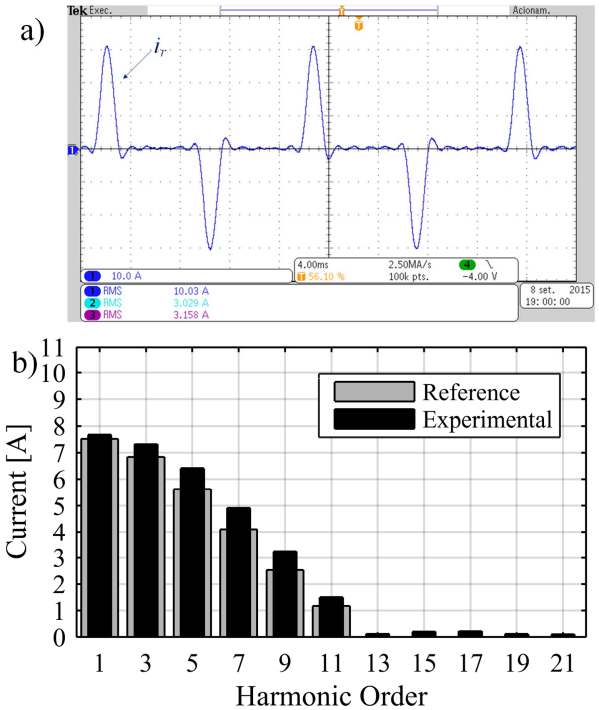

Fig. 13. Emulation of a single-phase capacitive rectifier input current. a) 10 Amperes RMS input current (10A/div, 4*ms*/div); b) Harmonic amplitudes comparison among experimental and single-phase capacitive rectifier reference currents.

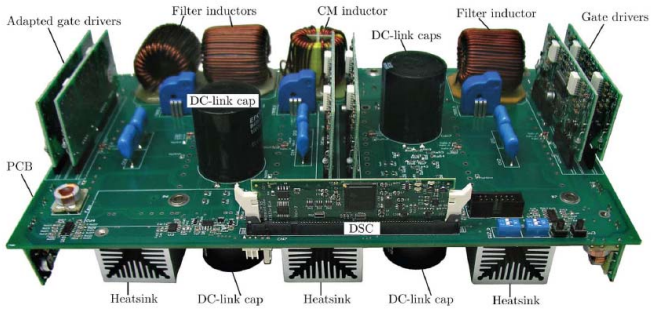

Fig. 14. Three-Phase T-NPC converter laboratory prototype.

VII. CONCLUSIONS

This paper presented a control strategy for a T-NPC interleaved converter in an AC active electronic load application. The simulation and experimental results showed that the strategy adopted gives active damping of LCL filter resonance and sensorless control with low ripple at the controlled EUT current. Besides, linear and nonlinear load emulation with high harmonic content is achieved, enabling control of high currents at high frequencies.

Although the current average value difference between phases, the proposed interleaving operation is achieved allowing high power density in an AC AEL single-phase application. To work around the problem and be able to achieve equal RMS value of currents even with different values of inductance, it is necessary to use a strategy that control the current phases independently, although with the disadvantage of increased complexity.

ACKNOLEDGEMENTS

The authors would like to thank UDESC, FITEJ and FAPESC for supporting the project.

REFERENCES

[1] C. Nan and H. S. H. Chung, "Energy-Recyclable Burn-In Technology for Electronic Ballasts," *Power Electronics, IEEE Transactions on,* vol. 26, pp. 2550-2562, 2011.

[2] R. Bojoi, E. Armando, S. G. Rosu, S. Vaschetto, and P. Soccio, "Virtual load with common mode active filtering for power hardware-in-the-loop testing of power electronic converters," in *Industrial Electronics Society, IECON 2014 - 40th Annual Conference of the IEEE*, 2014, pp. 1875-1881.

[3] W. Jing, M. Yiwei, Y. Liu, L. M. Tolbert, and F. Wang, "Power converter-based three-phase induction motor load emulator," in *Applied Power Electronics Conference and Exposition (APEC), 2013 Twenty-Eighth Annual IEEE*, 2013, pp. 3270-3274.

[4] M. H. Hedayati and V. John, "Circulating power test setup for a PWM rectifier motor drive," in *Power Electronics, Drives and Energy Systems (PEDES), 2012 IEEE International Conference on*, 2012, pp. 1-5.

[5] M. Yiwei, Y. Liu, W. Jingxin, F. Wang, and L. M. Tolbert, "Emulating full-converter wind turbine by a single converter in a multiple converter based emulation system," in *Applied Power Electronics Conference and Exposition (APEC), 2014 Twenty-Ninth Annual IEEE*, 2014, pp. 3042-3047.

[6] M. Thorne and M. Kazerani, "A regenerative controllable DC load for an electric vehicle test station," in *Industrial Electronics, 2009. IECON '09. 35th Annual Conference of IEEE*, 2009, pp. 3773-3778.

[7] C. Wenchao, M. Yiwei, W. Jingxin, Y. Liu, W. Jing, F. Wang*, et al.*, "Two-stage PV inverter system emulator in converter based power grid emulation system," in *Energy Conversion Congress and Exposition (ECCE), 2013 IEEE*, 2013, pp. 4518-4525.

[8] J. A. Heerdt, S. A. Mussa, and M. L. Heldwein, "Semiconductors current efforts and losses evaluation for single-phase three-level regenerative PWM rectifiers," in *Industrial Electronics (ISIE), 2010 IEEE International Symposium on*, 2010, pp. 1046-1051.

[9] M. Schweizer and J. W. Kolar, "Design and Implementation of a Highly Efficient Three-Level T-Type Converter for Low-Voltage Applications," *Power Electronics, IEEE Transactions on,* vol. 28, pp. 899-907, 2013.

[10] M. Liserre, F. Blaabjerg, and S. Hansen, "Design and control of an LCL-filter-based three-phase active rectifier," *Industry Applications, IEEE Transactions on,* vol. 41, pp. 1281-1291, 2005.

[11] R. W. Erickson, *Fundamentals of Power Electronics*. New York, EUA: Chapman & Hall, 1997.

[12] K. Ogatha, *Discrete-Time Control System*. New Jersey: Pretency Hall, 1994.

[13] W. Eric and P. W. Lehn, "Digital Current Control of a Voltage Source Converter With Active Damping of LCL Resonance," *Power Electronics, IEEE Transactions on,* vol. 21, pp. 1364-1373, 2006.

[14] J. Dannehl, F. W. Fuchs, and P. B. Thogersen, "PI State Space Current Control of Grid-Connected PWM Converters With LCL Filters," *Power Electronics, IEEE Transactions on,* vol. 25, pp. 2320-2330, 2010.

[15] G. Franklin and D. Powell, *Digital Control of Dynamic Systems*. California, EUA: Addison-Wesley Publishing Company, 1981.

[16] N. Hoffmann, M. Hempel, M. C. Harke, and F. W. Fuchs, "Observer-based grid voltage disturbance rejection for grid connected voltage source PWM converters with line side LCL filters," in *Energy Conversion Congress and Exposition (ECCE), 2012 IEEE*, 2012, pp. 69-76.

[17] S.-h. Wang, W.-y. Ju, Z.-l. Jia, and L. Peng, "Study on dual-loop control for inverters based on state observer with repetitive compensation," in *Power Electronics and Motion Control Conference, 2009. IPEMC '09. IEEE 6th International*, 2009, pp. 1550-1553.

[18] J. A. Heerdt, D. Ferreira Coutinho, S. A. Mussa, and M. Lobo Heldwein, "Control Strategy for Current Harmonic Programmed AC Active Electronic Power Loads," *Industrial Electronics, IEEE Transactions on,* vol. 61, pp. 3810-3822, 2014.